minerals

MDPI

Article

Crystal Chemistry of Chlormagaluminite, $Mg_4Al_2(OH)_{12}Cl_2(H_2O)_2$, a Natural Layered Double Hydroxide

Elena S. Zhitova [1,2,*], Sergey V. Krivovichev [1,3], Igor V. Pekov [4] and Vasiliy O. Yapaskurt [4]

[1] Department of Crystallography, Institute of Earth Sciences, St. Petersburg State University, University Emb. 7/9, 199034 St. Petersburg, Russia; s.krivovichev@spbu.ru;
[2] Institute of Volcanology and Seismology, Russian Academy of Sciences, Bulvar Piipa 9, 683006 Petropavlovsk-Kamchatsky, Russia
[3] Nanomaterials Research Centre, Kola Science Centre, Russian Academy of Sciences, Fersman Street 14, 184209 Apatity, Russia
[4] Department of Mineralogy, Faculty of Geology, Moscow State University, Leninskie Gory 1, 119991 Moscow, Russia; igorpekov@mail.ru (I.V.P.); yvo72@geol.msu.ru (V.O.Y.)
* Correspondence: zhitova_es@mail.ru

Received: 16 March 2019; Accepted: 6 April 2019; Published: 8 April 2019

Abstract: Chlormagaluminite is the only Cl-dominated hydrotalcite-supergroup mineral species with M^{2+}:M^{3+} = 2:1. The holotype sample of chlormagaluminite from the Kapaevskaya volcanic pipe (Irkutsk Oblast, Siberia, Russia) has been chemically and structurally characterized. The average chemical composition of the mineral is (electron microprobe, OH content is calculated by stoichiometry and H_2O from the crystal-structure data, wt. %): MgO 33.85, FeO 1.09, Al_2O_3 22.07, Cl 14.72, H_2O_{tot} 30.96, Cl=O −3.39, total 99.30. The empirical formula based on Mg + Al + Fe = 6 atoms per formula unit (*apfu*) is $[Mg_{3.91}Fe^{2+}_{0.07}Al_{2.02}(OH)_{12}]Cl_{2.02}(H_2O)_{2.0(2)}$. The crystal structure has been solved from single-crystal X-ray diffraction data in the space group $P6_3/mcm$, a = 5.268(3), c = 15.297(8) Å and V = 367.6(4) Å^3. The refinement converged to R_1 = 0.083 on the basis of 152 unique reflections with $I > 2\sigma(I)$ collected at room conditions. The powder pattern contains standard reflections of a 2*H* polytype and two additional reflections [(010), d_{010} = 4.574 Å; (110), d_{110} = 2.647 Å] indicative of Mg and Al ordering according to the $\sqrt{3}\times\sqrt{3}$ superstructure. The structure is based upon brucite-type octahedral layers with an ordered distribution of Mg and Al over octahedral sites. The Cl^- anions and H_2O molecules reside in the interlayer, providing a three-dimensional integrity of the structure.

Keywords: chlormagaluminite; layered double hydroxide; LDH; quintinite group; hydrotalcite supergroup; structure

1. Introduction

Chlormagaluminite, $Mg_4Al_2(OH)_{12}Cl_2(H_2O)_2$, is a member of the quintinite group, which belongs to the hydrotalcite supergroup [1]. Hydrotalcite-supergroup minerals and their synthetic analogs are known as layered double hydroxides (LDHs), which found many applications in modern industry. The structures of LDHs are built of positively charged brucite-type layers consisting of $[M^{2+}(OH)_6]$ and $[M^{3+}(OH)_6]$ octahedra. The metal-hydroxide layers are interstratified with interlayer anions and water molecules. Species-defining parameters [1] for hydrotalcite-supergroup minerals are as follows: (i) the dominant M^{2+} cation; (ii) the dominant M^{3+} cation; (iii) the dominant interlayer anion, and (iv) the M^{2+}:M^{3+} ratio with the values 2:1 and 3:1 being the most widespread among natural [1] and synthetic LDHs.

The chlorine-bearing LDHs are of special industrial interest because of their high anion-exchange capabilities. Therefore, they have been widely suggested for water purification [2–7] and for the immobilization of radionuclides [8,9]. It has been shown that Mg-Al-Cl LDHs form as secondary phases in leaching experiments with metallic uranium–aluminum research reactor fuel and may incorporate Eu into their structures [10]. They are endorsed for biosensors [11] and gas sensors [12]. In addition, the recent study demonstrated that the Mg_2Al-Cl (a synthetic analog of chlormagaluminite) and Zn_2Al-Cl LDHs can be applied for biomedical purposes due to their good compatibility with living matter [13]. Synthesis routes for the preparation of Mg-Al-Cl LDHs can be found in [14–20].

Chlormagaluminite was first described as "chlormanasseite" (named by analogy with the synthetic LDH) from a magnetite vein dissecting fine-grained pyroxene skarn in the drill core (Figure 1) extracted from a borehole at depths 1024.5 and 1024.6 m of the Kapaevskoe iron deposit related to the Kapaevskaya volcanic pipe located near Angara river (Irkutsk Oblast, Siberia, Russia) [21]. The mineral description was provided by Kashaev and coauthors [22,23] with the later paper [24] devoted to its single-crystal structure study. Although their structural study of chlormagaluminite [24] was incomplete in terms of localization of interlayer specie. Moreover, the previously proposed structural model (i.e., crystallographic information file (cif) file) [24] is unavailable in structural databases.

To date, chlormagaluminite is the only chlorine-dominated hydrotalcite-supergroup member with M^{2+}:M^{3+} = 2:1 (Mg_2Al-Cl LDH). Structural study of chlormagaluminite is of interest, since it may serve as a model type for natural and synthetic Cl-bearing LDHs.

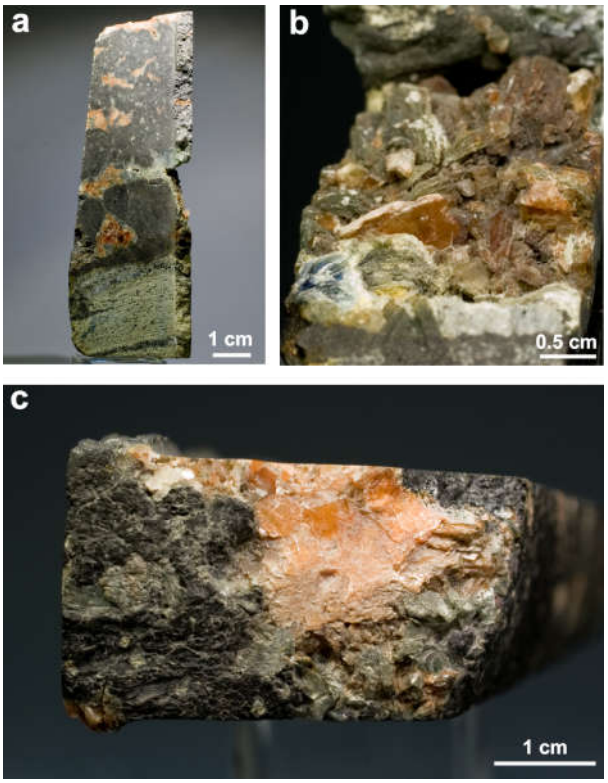

Figure 1. Photos of chlormagaluminite holotype specimen from the collection of Fersman Mineralogical Museum (catalogue number 82771): (**a**) a fragment of drill core consisting of a pyroxene skarn crosscut by a cavernous magnetite vein; chlormagaluminite crystals in the cavity (**b**), and at the core cut (**c**). Photo: M.M. Moiseev.

Previous Crystal Structure Determinations

The single-crystal structure refinement of chlormagaluminite was first undertaken by Kashaev and coauthors [24] (Table 1). These authors noticed the presence in X-ray diffraction patterns of weak inconsistent (and irregular) reflections that were attributed to the appearance of thin films of a newly formed phase on the surface of single crystals during X-ray data collection. In addition, they reported that the newly formed phase appeared on air and disappeared when crystals were annealed at temperature 100 to 120 °C for 3 to 4 h or held in a vacuum. Nevertheless, their study allowed for the identification of the structure model of chlormagaluminite visualized in Figure 2. The specific feature of this model is the ordering of Mg^{2+} and Al^{3+} cations according to the $\sqrt{3}\times\sqrt{3}$ superstructure. However, the authors experienced considerable difficulties in localizing interlayer anions. In general, the structure model proposed by them [24] is crystal chemically reasonable with the exception of localization of the Ow2 (interlayer) atom which is too far from the potential position of H atom of the metal-hydroxide layer (Figure 2c).

Table 1. Crystallographic data and refinement parameters reported for chlormagaluminite, its synthetic Zn-analog, and for synthetic Al-analog of iowaite.

Species	**Chlormagaluminite**	**Synthetic Zn-analogs of Chlormagaluminite**		**Synthetic Al-analog of Iowaite**
Chemical formula	$[Mg_4Al_2(OH)_{12}][Cl_2(H_2O)_2]$	$[Zn_4Al_2(OH_{12}][Cl_2(H_2O)_4]$	$[Zn_{3.9}Al_{2.1}(OH)_{12}][Cl_{2.1}(H_2O)_{2.1}]$	$[Mg_6Al_2(OH)_{16}][Cl_{1.76}(CO_3)_{0.12}(H_2O)_{4.8}]$
Refinement	Single-crystal XRD data, direct method	Rietveld-Le Bail refinement	Rietveld refinement and MD-simulation	Rietveld refinement
Symmetry	Hexagonal	Trigonal	Trigonal	Trigonal
Space group	*P*-6*c*2 [3]	*R*-3*m*	*R*-*m* [4]	*R*-3*m*
a, Å	5.280(2)	3.083	3.07497(6)	3.0649(7)
b, Å	=*a*	=*a*	=*a*	=*a*
c, Å	15.344(6)	23.47	23.1524(5)	23.913(9)
V, Å^3	374.67	193.19 [5]	189.588(6)	194.53 [5]
Z	1	1	1	1
Density, g/cm^3	2.06 [5]/2.067 [6]	2.848 [6]	2.759 [5]/2.751 [6]	1.881 [5]/2.07 [6]
Number of reflections	121	n.g.	n.g.	n.g.
R_1	0.083	4.95	0.076	n.g.
R_w	0.088	13.25	0.119	n.g.
Polytype	2*H*	3*R*	3*R*	3*R* (3R_1)
a`, Å [1]	3.05	3.09	3.08	3.06
d, Å [2]	7.73	7.85	7.72	7.97
Source	[24]	[25]	[26]	[9]

[1] *a*` the distance between two adjacent *M*–*M* cations in metal-hydroxide layer (equal to the *a* parameter if no long-range order is observed); [2] the layer spacing d_{00n} of *n*-layer polytype; [3] other space groups used for refinement are $P6_3/mcm$ and $P6_3cm$; [4] corrected to *R*-3*m* from *R*3*m* given in the paper (because the space group *R*3*m* does not produce the octahedral layers using reported atom coordinates); [5] originally given value; [6] recalculated here value as $D = (M \times Z)/(V \times N_A)$, *D*—density; *M*—molar mass; *Z*—number of formula units; N_A—Avogadro constant; n.g.—not given.

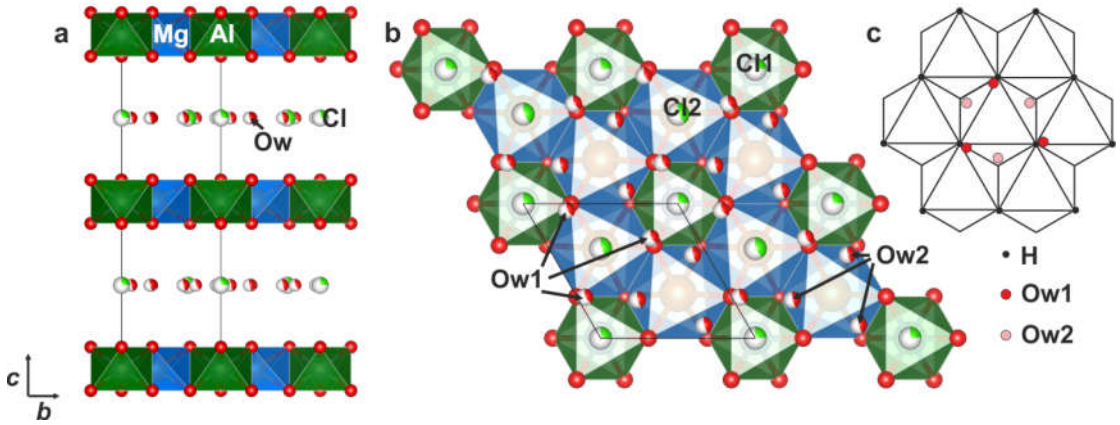

Figure 2. Projections of structure model proposed for chlormagaluminite by Kashaev and coauthors [24]: (**a**) along *z*; (**b**) within *xy* plane, and (**c**) position of interlayer Ow1 and Ow2 (z = 1/4) atoms relative to the hypothetic position of H atoms (z ~ 0.12) of the metal-hydroxide layer.

Structure characteristics of synthetic chlorine-bearing LDHs obtained by the Rietveld structure refinements were given for Zn-analogs of chlormagaluminite [25,26] and for chlorine-bearing LDHs with M^{2+}:M^{3+} = 3:1 [27], i.e., iowaite-like species (Table 1). Their structure models are schematically represented in Figure 3 from which it can be concluded that localization of interlayer anion is still a challenging issue in the structure determination of Cl-bearing LDHs.

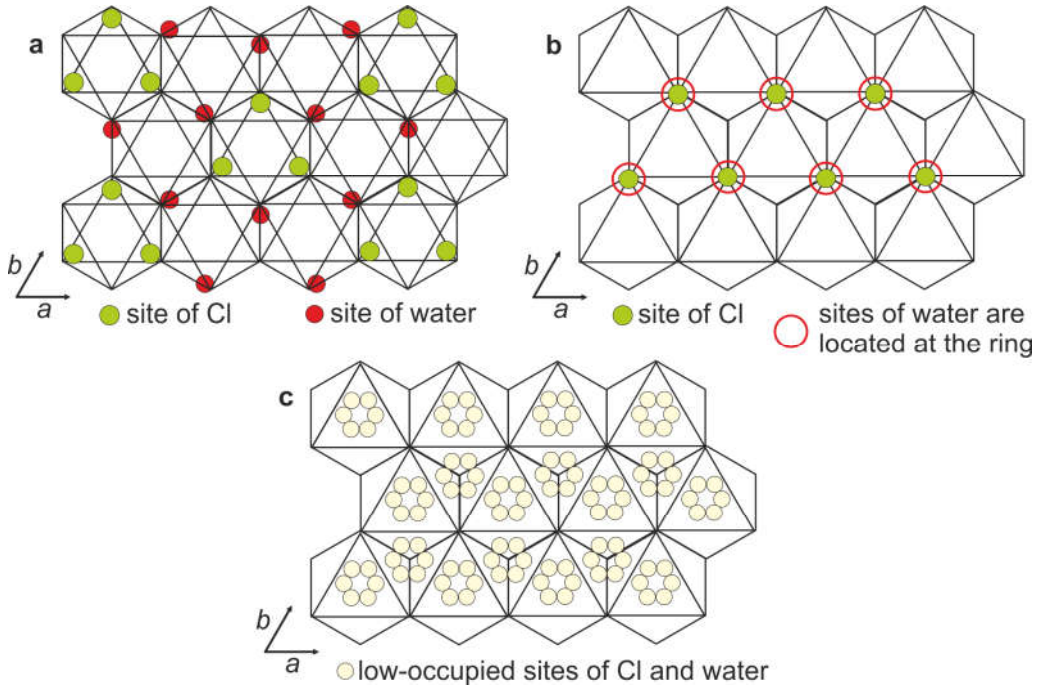

Figure 3. Structural model suggested for chlorine-bearing LDHs by (**a**) [9]; (**b**) [25] and (**c**) [26]. Note that interlayer sites are low-occupied.

2. Materials and Methods

2.1. Sample Description

In this study, we reinvestigated the type specimen of chlormagaluminite deposited in the systematic collection of the Fersman Mineralogical Museum of the Russian Academy of Sciences

(Moscow) under catalog number 82771. This specimen (Figure 1a) is a fragment of drill core consisting of a pyroxene skarn crosscut by a cavernous magnetite vein. The cavities (up to 3 cm across) contain aggregates of pale-greenish clinochlore and yellow-brown chlormagaluminite. The latter occurs as hexagonal lamellar and dipyramidal crystals up to 0.5 cm in size overgrowing clinochlore and earlier magnetite. Some cavities are almost completely filled by lamellar aggregates of chlormagaluminite. This mineral is transparent, colorless or light yellow to yellow-brown (Figure 1b,c).

2.2. Chemical Composition

The chemical composition of chlormagaluminite was studied using a JEOL JSM-6480LV scanning electron microscope (JEOL, Tokyo, Japan) equipped with an INCA-Wave 500 wavelength-dispersive spectrometer (Laboratory of Analytical Techniques of High Spatial Resolution, Dept. of Petrology, Moscow State University, Moscow, Russia). The wavelength-dispersive spectroscopy (WDS)mode was used, with an acceleration voltage of 20 kV and a beam current of 10 nA; the electron beam was rastered to 5 μm × 5 μm area to minimize damage to the sample. The standards used are as follows: MgO (Mg), Al_2O_3 (Al), Fe (Fe), and NaCl (Cl). Contents of other elements with atomic numbers higher than oxygen are below detection limits. No chemical zoning was observed in the studied crystals.

2.3. Infrared Spectroscopy (IR)

The IR spectrum of chlormagaluminite was recorded using a Bruker Vertex IR spectrometer (Bruker, Billerica, MA, USA). The measurements were taken at room temperature using the KBr technique.

2.4. Single-Crystal X-ray Diffraction

Numerous crystals from the sample 82771 were checked using different single-crystal X-ray diffraction machines, which were used to collect diffraction datasets. Similar to Kashaev and coauthors [24], we have observed the presence of weak inconsistent (irregular) reflections at diffraction patterns of each studied sample. Among studied crystals, we have found one suitable enough for the collection of a more or less reliable dataset. The experiment was carried out with Mo$K\alpha$ radiation by means of a Bruker Apex II Duo diffractometer (Bruker, Billerica, MA, USA) operated at 50 kV/40 mA and equipped with a charge coupled device (CCD) area detector. The intensity data were reduced and corrected for Lorentz, polarization, and background effects using Bruker software Apex2 [27]. The CrysAlis PRO program was also used for data processing [28]. A semi-empirical absorption-correction based upon the intensities of equivalent reflections was applied (SADABS, [27,29]). The unit-cell parameters were refined by the least-squares methods. The SHELX program package was used for all structural calculations [29]. Crystal structures were visualized using the Vesta program [30].

The problem of the presence of inconsistent reflections is not entirely new for hydrotalcite-supergroup minerals due to crystal imperfections, e.g., [31]. However, in the present study, even the best-quality crystal produced an essential number of such reflections, which was also typical for all studied samples. Although the formation of a new phase as suggested by Kashaev and coauthors [24] would explain the problems with the data collection, we cannot confirm or deny its appearance and, therefore, are unable to comment on the nature of the observed inconsistent reflections. The influence of the weak inconsistent reflections is reflected by the slightly high value of R_{int} = 7% and crystallographic agreement indices. However, the structure model was crystal chemically reasonable, though perhaps not absolutely perfect.

2.5. Powder X-ray Diffraction

Several crystals of chlormagaluminite were crushed and mounted in Paraton oil in a loop. The sample was studied by Gandolfi-like measurements by means of a Rigaku R-AXIS Rapid II

single-crystal diffractometer (Rigaku, Tokyo, Japan) equipped with a cylindrical image plate detector using Debye–Scherrer geometry (d = 127.4 mm; Co$K\alpha$). The data were converted using osc2xrd program [32]. Topas 4.2 [33] was used for the refinement of the unit-cell parameters of chlormagaluminite by the Pawley method and for indexing the powder X-ray diffraction data. The structural model obtained from single-crystal data was used.

The powder X-ray diffraction has been undertaken to check the homogeneity of samples in terms of possible intergrowth of visually undistinguishable phases or polytypes.

3. Results

3.1. Chemical Composition

The major elements with $Z > 6$ are Mg, Al, O, and Cl, with admixed Fe (Table 2) which was considered as Fe^{2+} due to the existence of a negative correlation between Mg and Fe. This composition is in agreement with the data reported for chlormagaluminite previously [22,23] and with the iron oxidation state in quintinite [34], which is a carbonate analog of chlormagaluminite. The hydroxyl groups were taken as two per cation in agreement with the LDHs stoichiometry, in particular, other quintinite-group minerals [1]. The molecular water content was calculated from the structure refinement from the site-scattering factors of sites at the interlayer level. The interlayer anion site is entirely occupied by Cl (both from the chemical composition and structure-refinement data). The presence of hydrogen in the form of both OH groups and H_2O molecules was confirmed by infrared (IR) spectroscopy and structure refinement (see below).

Table 2. Chemical composition of chlormagaluminite averaged for 15 analyses.

Constituent	Wt.%	Range (Stand. Dev.)	Constituent	*apfu*	Range
			Formula calculated on the basis of Mg + Al + Fe = 6 *apfu*		
MgO	33.85	33.07–34.76 (0.32)	Mg	3.91	3.87–3.96
FeO	1.09	0.55–1.96 (0.38)	Fe	0.07	0.04–0.12
			ΣM^{2+}	4.98	
Al_2O_3	22.07	21.16–22.83 (0.24)	Al	2.02	2.00–2.01
			ΣM^{3+}	2.02	
H_2O_{tot}[(1),(2)]	30.96		OH [1]	12	
			H_2O [2]	2.0	
Cl	14.72	11.95–16.25 (1.32)	Cl	1.97	1.70–2.14
-Cl=O	−3.39				
Total	99.30		M^{2+}/M^{3+}	2.0	

[1] Amount of hydroxyl groups located in metal-hydroxide layer is calculated by stoichiometry: $2(OH)^-$ per cation; [2] Interlayer water content is calculated from structure refinement (as 2.0 *apfu*, see below).

3.2. Infrared Spectroscopy (IR)

The IR spectrum of chlormagaluminite is shown in Figure 4. The band assignment is given in Table 3. The main feature of the spectrum is the presence of intensive bands in the O–H stretching (3600–3400 cm^{-1}) and H–O–H bending regions around (1800 and 1610 cm^{-1}). The band with a maximum at 858 cm^{-1} is assigned as corresponding to Al···O–H, Mg···O–H bending vibrations involving OH groups forming strong hydrogen bonds with O atoms. The bands with frequencies below 700 cm^{-1} were assigned to the lattice modes. It is noteworthy that the bands assignable to carbonate-ion vibrations are absent in the spectrum implying the absence of carbonate groups in the mineral.

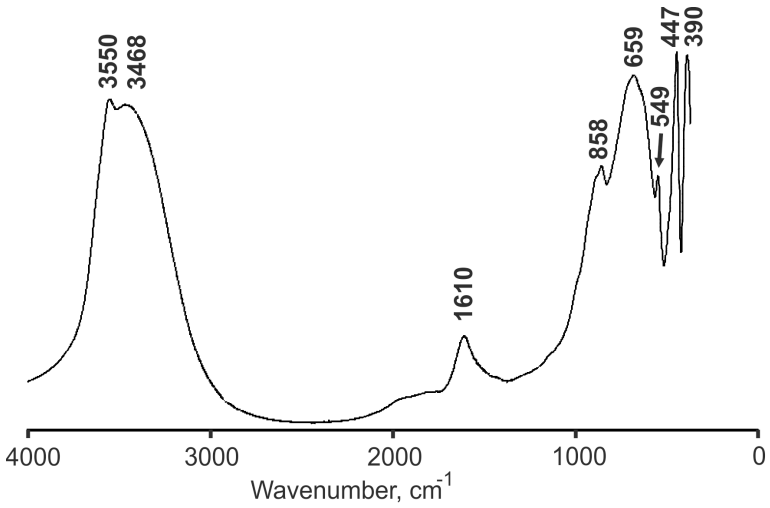

Figure 4. Infrared (IR absorption) spectrum of chlormagaluminite.

Table 3. Assignment of infrared (IR) bands (cm^{-1}) of chlormagaluminite and its comparison to quintinite.

Chlormagaluminite	Quintinite [34]	Quintinite [35]	Assignment
3550 3432	- 3437	- 3388	O–H stretching
-	~3100–2700 sh	3184, 3029	interaction of interlayer water and carbonate-ion
1800 sh 1610	1750–1500 sh	1571	H–O–H bending
- -	~1400 sh 1355	1407 1350	Antisymmetric stretching of carbonate
-	960–940 sh	949	v_2 bending of carbonate
858	880–860 sh	866, 841	Al···O–H, Mg···O–H bending vibrations involving OH groups forming strong hydrogen bonds with O atoms
-	783	776	v_4 bending of carbonate
679 549 447 390	679 552 449 393	673 n.r. n.r. n.r.	Lattice modes

n.r.—not reported.

3.3. Single-Crystal X-ray Diffraction

The single-crystal X-ray diffraction data were initially indexed in the trigonal unit cell, space group *P*-3*c*1. The positions of atoms in the metal hydroxide layer were determined in the space group *P*-3*c*1. The test for a higher symmetry applying the Platon program [36] indicated the $P6_3/mcm$ space group (Table 4). The interlayer atoms and hydrogen atoms of the metal-hydroxide layer were added to the refinement after the structure transformation to the $P6_3/mcm$ space group. Site occupancies of the Mg, Al, and O atoms of the metal-hydroxide layer were found to be close to 100 % and, therefore, fixed, while site occupancies of the interlayer atoms were refined. No restraints (and constraints) were applied during the refinement of the positions of H atoms of the metal-hydroxide layers, because their positions were easily observed from the electron-density difference Fourier maps and the refined O–H distances of 0.92 Å appeared to be trustworthy. The equivalent isotropic displacement parameter of the H atom has been fixed. Anisotropic displacement parameters were refined only for Mg, Al, and O of the metal-hydroxide layer and for the rest of atoms isotropic

approximation was used. Atom coordinates, site occupancies, and displacement parameters are given in Table 5. Selected interatomic distances are provided in Table 6. The crystallographic information file has been deposited with the Editors and is available as Supplementary Material (see below).

Table 4. Crystal data, data collection, and structure refinement details for chlormagaluminite.

Crystal Chemical Data	
Crystal system	Hexagonal
Space group	$P6_3/mcm$
a, (Å)	5.268(3)
c, (Å)	15.297(8)
Unit-cell volume (Å^3)	367.6(4)
Z	1
Calculated density (g/cm^3)	2.07
Absorption coefficient	0.871
Data Collection	
Diffractometer	Bruker APEX II DUO
Temperature (K)	293(2)
Radiation, wavelengths (Å)	Mo $K\alpha$, 0.71073
Range for data collection, θ (°)	2.66–33.35
h, *k*, *l* ranges	−8→6, −7→5, −23→19
Total reflections collected	277
Unique reflections (R_{int})	0.0701
Number of unique reflections $F > 2\sigma(F)$	152
Data completeness (%)	95.5
Structure Refinement	
Refinement method	Full-matrix least-squares on F^2
Weighting coefficients *a*, *b*	0.117800, 0
Data/ restraints/ parameters	277/0/33
R_1 [$F > 2\sigma(F)$], wR_2 [$F > 2\sigma(F)$]	0.0826, 0.1954
R_1 all, wR_2 all	0.1207, 0.2181
Goodness-of-fit on F^2	1.093
Largest diff. peak and hole (ēÅ^{-3})	0.53, 0.29

Table 5. Atom coordinates, equivalent isotropic displacement parameters (Å^2), site occupancies, and assigned site populations for chlormagaluminite.

Atom	**W.P.**	***x***	***y***	***z***	U_{eq}	**s.o.f**	**s.s. ref (ē)**	**Assigned Site Population**
Octahedral layer								
Mg1	4d	1/3	2/3	0	0.0167(8)	1*	48	Mg_4
Al1	2b	0	0	0	0.0161(9)	1*	26	Al_2
O1	12k	0.3094(5)	0.3094(5)	0.0644(2)	0.0154(8)	1*	96	$(OH)_{12}$
H1	12k	0.294(8)	0.294(8)	0.124(4)	0.02*	1*	12	
Interlayer gallery								
Cl1	12j	0.739(8)	0.338(12)	1/4	0.022(3)	0.044(6)	9(1)	$Cl_{2.2(3)}$
Cl2	6g	0	0.054(5)	1/4	0.020(1)	0.080(5)	8.2(7)	
Cl31	12j	0.335(5)	0.089(5)	1/4	0.040(8)	0.077(12)	16(2)	
Cl32	6g	0.39(2)	0	1/4	0.06(3)	0.05(2)	5(2)	
O2w	12j	0.408(6)	0.319(6)	1/4	0.07(2)	0.18(2)	16(2)	$(H_2O)_{2.0(2)}$

* fixed during refinement; W.P.—Wyckoff position.

Table 6. Selected bond lengths (Å) and angles (°) in the crystal structure of chlormagaluminite.

Octahedral layer			
Mg–O	2.071(2) × 6	Al–O	1.904(3) × 6
Interlayer gallery			

Interlayer prism 1		Interlayer prism 2		Interlayer prism 3	
Cl1–H1(a)	2.59(6) × 4	Cl2–H1(a)	2.42(5) × 4	Cl31–H1(a)	2.28(5) × 2
Cl1–H1(b)	2.96(6) × 2	Cl2–H1(b)	2.68(5) × 2	Cl31–H1(b)	2.73(5) × 2
<Cl1–H1>	2.71	<Cl2–H1>	2.51	Cl31–H1(c)	2.95(5) × 2
				Cl32–H1(a)	2.55(8) × 2
				Cl32–H1(b)	2.69(7) × 4
				<Cl3–H1>	2.64

Hydrogen bonding scheme

D–H	d(D–H)	d(H..A)	<DHA	d(D..A)	A
O1–H1	0.917	2.952	127.76	3.587	Cl1
O1–H1	0.917	2.570	136.27	3.294	Cl1
O1–H1	0.917	2.585	134.47	3.293	Cl1
O1–H1	0.917	2.952	127.76	3.587	Cl1
O1–H1	0.917	2.399	148.30	3.215	Cl2
O1–H1	0.917	2.659	141.39	3.424	Cl2
O1–H1	0.917	2.271	149.48	3.096	Cl31
O1–H1	0.917	2.943	126.00	3.560	Cl31
O1–H1	0.917	2.709	138.15	3.446	Cl31
O1–H1	0.917	2.678	137.18	3.408	Cl32
O1–H1	0.917	2.540	134.37	3.247	Cl32
O1–H1	0.917	2.003	160.49	2.883	O2W

3.4. Powder X-ray Diffraction

Indexed powder X-ray diffraction data are provided in Table 7 with the Pawley fit shown in Figure 5. The phase analysis indicated a good agreement between our data and JCPDS-ICDD card # 00-038-0446 of chlormagaluminite based on the data from [24] (Table 7), although reflections of low intensity have not been registered previously. The unit-cell parameters refined from the powder X-ray diffraction data are a = 5.2857(1), c = 15.4323(5) Å that are very close to those reported originally for the type specimen: a = 5.29, c = 15.46 Å [22,23]. The powder pattern contains strong reflections corresponding to a hexagonal stacking sequence, i.e., to a 2*H* polytype. At the same time, it contains two superstructure reflections: (010) and (110) indicative of cation ordering in the metal-hydroxide layer and the formation of the $\sqrt{3}\times\sqrt{3}$ superstructure (in the xy plane) (Figure 5).

Table 7. Powder X-ray diffraction data for chlormagaluminite.

This work						**JCPDS-ICDD card # 00-038-0446 [24]**	
I_{rel} (%)	d_{meas} (Å)	d_{calc} (Å)	h	k	l	d_{meas} (Å)	I_{rel} (%)
100	**7.72**	**7.72**	**0**	**0**	**2**	**7.67**	**100**
5	4.574	4.577	0	1	0	4.55	20
5	3.891	3.937	0	1	2	n.r.	n.r.
38	**3.856**	**3.858**	**0**	**0**	**4**	**3.86**	**80**
2	2.988	2.950	0	1	4	n.r.	n.r.
2	2.642	2.643	1	1	0	n.r.	n.r.
12	2.603	2.605	1	1	1	2.60	80
3	2.571	2.572	0	0	6	n.r.	n.r.
12	2.499	2.500	1	1	2	2.49	70
38	**2.350**	**2.351**	**1**	**1**	**3**	**2.34**	**90**
1	2.287	2.289	0	2	0	n.r.	n.r.
1	2.240	2.242	0	1	6	n.r.	n.r.
34	**2.179**	**2.180**	**1**	**1**	**4**	**2.17**	**90**
17	2.007	2.007	1	1	5	2.00	60
1	1.930	1.929	0	0	8	n.r.	n.r.
29	**1.843**	**1.843**	**1**	**1**	**6**	**1.839**	**100**
1	1.716	1.719	2	1	1	n.r.	n.r.
		1.710	0	2	6		

1	1.693	1.693	1	1	7	n.r.	n.r.
		1.688	2	1	2		
2	1.639	1.640	2	1	3	n.r.	n.r.
16	1.558	1.558	1	1	8	1.555	80
13	1.525	1.526	0	3	0	1.526	90
2	1.500	1.509	2	1	5	n.r.	n.r.
13	1.496	1.497	0	3	2	1.496	90
<1	1.475	1.475	0	2	8	n.r.	n.r.
1	1.439	1.438	1	1	9	n.r.	n.r.
		1.435	2	1	6		
4	1.419	1.419	0	3	4	1.417	40
5	1.332	1.332	1	1	10	1.330	40
2	1.321	1.321	2	2	0	n.r.	n.r.
<1	1.315	1.316	2	2	1	n.r.	n.r.
		1.312	0	3	6		
1	1.302	1.302	2	2	2	1.302	30
1	1.286	1.288	2	1	8	n.r.	n.r.
		1.286	0	0	12		
1	1.279	1.280	2	2	3	1.281	30
		1.279	0	2	10		
<1	1.269	1.269	3	1	0	n.r.	n.r.
		1.265	3	1	1		
3	1.250	1.253	3	1	2	1.250	40
		1.250	2	2	4		
1	1.239	1.239	1	1	11	n.r.	n.r.
		1.238	0	1	12		
1	1.233	1.232	3	1	3	2.237	20
1	1.214	1.218	2	1	9	2.217	10
		1.215	2	2	5		
<1	1.200	1.200	0	3	8	n.r.	n.r.
4	1.175	1.175	2	2	6	1.175	60
		1.174	3	1	5		
2	1.156	1.156	1	1	12	1.155	50
<1	1.150	1.152	2	1	10	n.r.	n.r.
<1	1.143	1.144	0	4	0	n.r.	n.r.
<1	1.137	1.138	3	1	6	n.r.	n.r.
<1	1.133	1.133	2	2	7	n.r.	n.r.
		1.132	0	4	2		
<1	1.102	1.102	0	0	14	n.r.	n.r.
		1.100	3	1	7		
5	1.090	1.090	2	2	8	1.091	60
		1.090	2	1	11		
1	1.083	1.085	0	3	10	n.r.	n.r.
		1.083	1	1	13		

n.r.—not reported; the strongest X-ray powder-diffraction (XRD) lines are bolded.

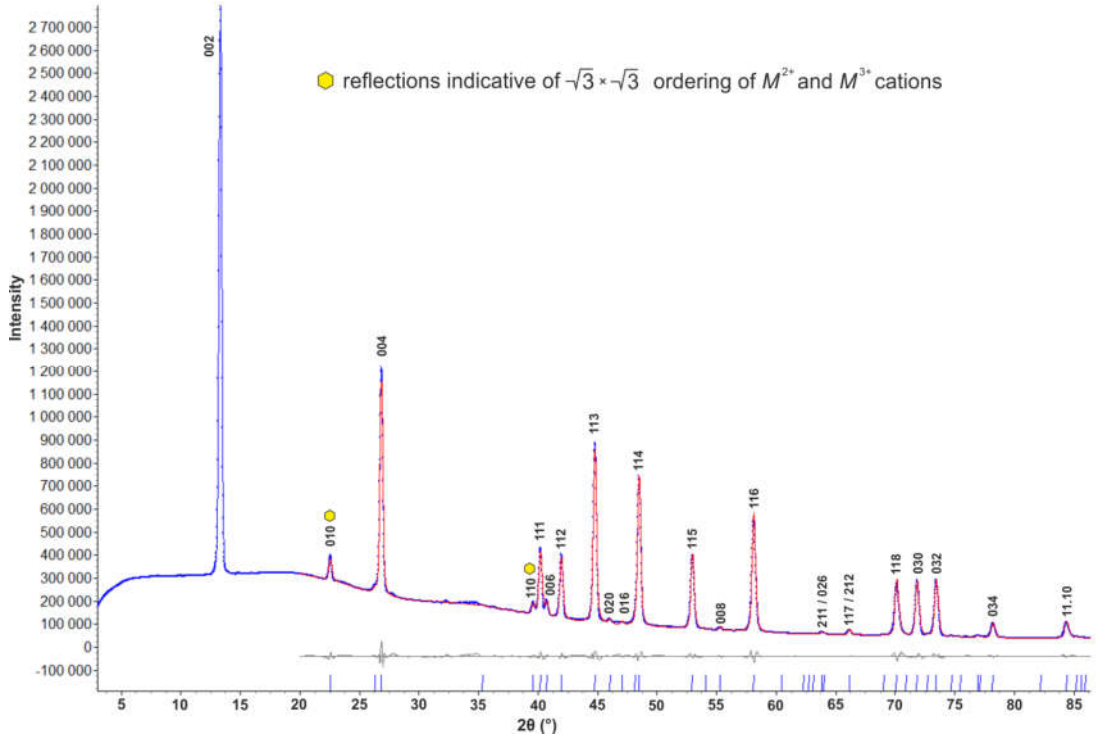

Figure 5. Indexed powder XRD pattern of chlormagaluminite: Pawley fit between experimental (blue) and calculated (red) lines. The reported here structure model is applied; superstructure reflections are marked.

4. Discussion

4.1. Chemical Composition

The chemical composition of chlormagaluminite studied here, $[Mg_{3.91}Fe_{0.07}Al_{2.02}(OH)_{12}]Cl_{2.02}(H_2O)_{2.0}$, slightly differs from the original data for the holotype specimen, $[Mg_{3.55}Fe^{2+}_{0.27}Na_{0.05}Al_{1.93}Fe^{3+}_{0.07}Ti_{0.01}(OH)_{12}]Cl_{1.48}(CO_3)_{0.12}(H_2O)_{2.42}$ [22,23]. It is worth noting that some variations in the Mg/Fe ratio have been observed in the earlier studies [21] sine FeO content ranged from 1.92–1.95 wt. % [in pure (as authors refer) crystal from sample 5948] to 4.10 wt. % (crystals from sample 5949) what may explain some discrepancies between our and earlier chemical analyses. However, the simplified formula is sustained in both studies. No carbonate groups could be confirmed by the IR spectroscopy measurements. Taking into account that the sample was stored (in the Fersman Museum) in air, no bulk carbonatization of chlormagaluminite during its storage over 35 years was observed. The same feature was observed in our study of iowaite, $[Mg_6Fe^{3+}_2(OH)_{16}]Cl_2(H_2O)_4$, from Terektinsky range, another Cl-bearing LDH [36]. Although the formation of thin films of a new carbonate-bearing phase on tiny single-crystals during XRD experiments [24] cannot be denied, we have found no indication of this effect in our study. It is noteworthy that, in iowaite, $[Mg_6Fe^{3+}_2(OH)_{16}]Cl_2(H_2O)_4$, some of interlayer Cl^- ions may be substituted by OH^- groups (and not by CO_3^{2-} group) [37,38], and the same substitution scheme could be expected for chlormagaluminite and other Cl-bearing LDHs.

It should be noted that Cl-dominant hydrotalcite-supergroup members are usually found during borehole drilling (chlormagaluminite [21]; iowaite [39], and woodallite [40]). They have also been found in the mines (again at shallow depths, i.e., hundreds of meters or few kilometers), e.g., iowaite from Palabora mine, Transvaal, South Africa [38], from Udachnaya kimberlite pipe, Yakutia [41], from Korshunovskoye deposit [42], and from Talnakh, Norilsk district ([43] and our data, all Siberia, Russia. Thus, Cl-dominant natural layered double hydroxides may be rather abundant at shallow depths, where the access of atmospheric CO_2 is negligible. At the same time, iowaite with

high Cr content (that is genetically different from those mentioned above) may be found at the surface, i.e., in serpentinites of the ophiolitic and greenstone belts, characterized by a high content of Cr [37,44].

4.2. X-ray Crystallography and Crystal Structure

The agreement between our and previously reported X-ray diffraction data [22–24] is very good: the sample is a 2*H* polytype, the unit-cell parameters are very similar (see above), and the presence of the in-plane superstructure was confirmed in both studies through the observation of additional reflections (Table 7, Figure 5).

The crystal structure of chlormagaluminite (Figure 6) consists of (i) metal hydroxide layers with the composition $[Mg_2Al(OH)_6]$ and (ii) interlayer species with the composition $[Cl_2(H_2O)_2]$. There are two symmetrically independent cation sites (Table 5) in the metal-hydroxide layer that differ by the *M*–O bond lengths (Table 6): the site with longer bonds (2.071(6) Å) was assigned to Mg and the site with shorter bonds (1.904(3) Å) was assigned to Al. The Mg and Al atoms are ordered according to the $\sqrt{3}\times\sqrt{3}$ superstructure within metal-hydroxide layers, i.e., each M^{3+} (Al) is surrounded by six M^{2+} (Mg) (Figure 6), whereas each M^{2+} cation is surrounded by four M^{2+} and two M^{3+} cations. The metal-hydroxide layers are packed according to the hexagonal stacking sequence forming two-layer unit cell, with the polytype notation 2*H* [45]. The localization of interlayer species obeys charge distribution of the metal-hydroxide layers and the geometry of interlayer anions. In all 2*H*-LDHs, the interlayer space can be divided into trigonal prisms formed by H atoms of metal-hydroxide layers located above and below the interlayer level [46]. For chlormagaluminite-2*H* studied here, there are three types of such prisms corresponding to three types H atoms that refer to the $(OH)Mg_3$, $(OH)Al_3$, and $(OH)Mg_2Al$ configurations (Figures 6 and 7). The chlorine atoms are located near the centers of the prisms, whereas H_2O molecules are located around the middle points of the edges of the prisms (Figure 7). The interlayer Cl and Ow (O of H_2O) sites are statistically disordered, which is manifested by their low occupancies. There are two sets of distances between the O1 atom [or the H1 atom] of the octahedral layer and the interlayer species (Cl and Ow): (i) ~ 3.0 Å [2.0–2.1 Å] that refer to the O1–Ow [H1–Ow] contacts and ii) ~ 3.0–3.5 Å [2.2–2.8 Å] corresponding to the O1–Cl [H1–Cl] contacts (Table 6). The number of electrons (*epfu*) calculated for the group (ii) coincides with the chlorine content determined by the chemical analyses (Table 5), which prompted us to assign the group (i) sites to H_2O molecules only.

The crystal-structure model proposed here is different from those reported previously [9,24–26], although the model suggested by Kashaev and coauthors [24] (Figure 3) is close but incomplete. It is of interest that the $\sqrt{3}\times\sqrt{3}$ superstructure ordering of Mg and Al atoms was successfully registered by both single-crystal and powder X-ray diffraction in this and previous [22–24] studies. Thus, the presence of the reflection with d = 4.57 Å in the powder pattern of pure LDHs having M^{2+}:M^{3+}= 2:1 is a reliable indicator of cation ordering similar to the Li_2Al LDHs [47–50]. In contrast to Cl-bearing hydrotalcite-supergroup members, the carbonate species have been structurally characterized in more details including recent single-crystal or Rietveld structure refinements of hydrotalcite [31], pyroaurite [51–53], quintinite [34,53–58], takovite [59], and zaccagnaite [60]. It has been found that C atoms of CO_3 groups occupy central parts of the interlayer prisms (Figure 7b), whereas O atoms of CO_3 groups and H_2O molecules are disordered around the middle points of the prism edges. Therefore, in the case of carbonate LDHs, the position of H_2O molecules cannot be distinguished from the O atoms of CO_3 groups, which results in higher degree of interlayer disordering compared to the chlorine-bearing LDHs (Figure 7). This underlines the fundamental difference in the structure of the interlayer space of carbonate- and chlorine-bearing LDHs with M^{2+}:M^{3+}= 2:1 (quintinite-group members and their synthetic analogs), whereas the structure of the octahedral layers is essentially the same.

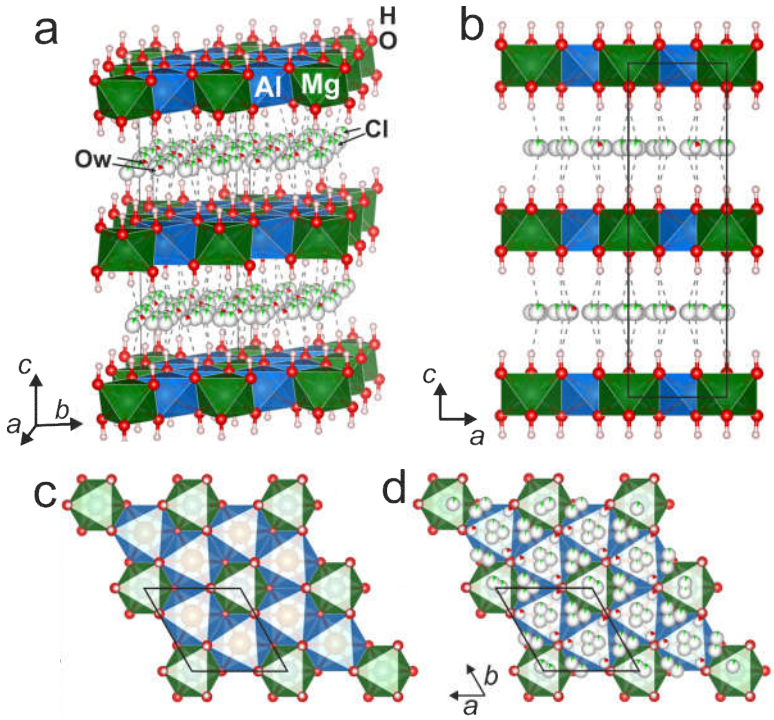

Figure 6. Projections of the crystal structure of chlormagaluminite: (**a**) general view; (**b**) hexagonal stacking sequence of metal-hydroxide layers; (**c**) ordering of Mg and Al according to $\sqrt{3}\times\sqrt{3}$ superstructure; (**d**) interlayer superimposed to metal-hydroxide layer.

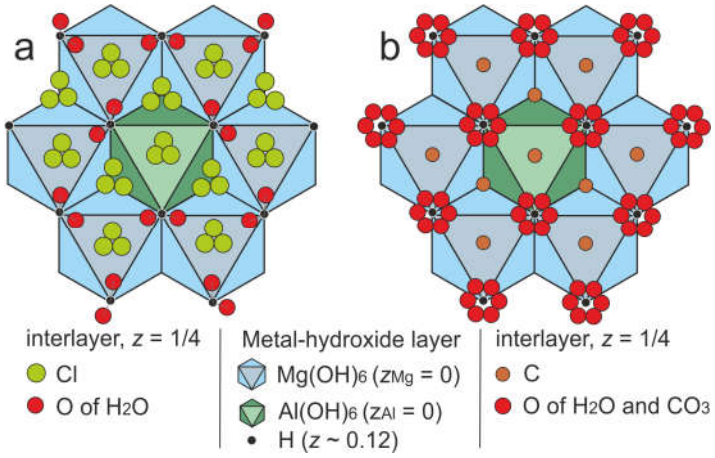

Figure 7. Interlayer arrangement of (**a**) chloride and (**b**) carbonate LDHs with M^{2+}:M^{3+} = 2:1 on the example of chlormagaluminite and quintinite [34].

5. Conclusions

The reinvestigation of the holotype sample of chlormagaluminite indicated rather good agreement between our and previous [22–24] studies in terms of crystal structures and chemistry and both agree with the following ideal chemical formula of the mineral, $[Mg_4Al_2(OH)_{12}]Cl_2(H_2O)_2$. The study reports the first single-crystal refinement of Cl-dominant quintinite-group member. The interlayer arrangement of chloride LDHs with M^{2+}:M^{3+} = 2:1 is different from that of carbonate varieties.

Supplementary Materials: The crystallographic information file (cif) is available online at www.mdpi.com/xxx/s1.

Author Contributions: Conceptualization, E.S.Z. and S.V.K.; Methodology, E.S.Z, S.V.K., and I.V.P.; Investigation, E.S.Z, I.V.P. and V.O.Y; Writing—Original Draft Preparation, E.S.Z., S.V.K. and I.V.P.; Writing—Review and Editing, E.S.Z., S.V.K., I.V.P. and V.O.Y.; Visualization, E.S.Z.

Funding: The study was supported by the Russian Science Foundation through the project 17-77-10023 (for E.S.Z.).

Acknowledgments: The study was carried out using facilities of XRD Resource Centre of St. Petersburg State University. We thank Fersman Mineralogical Museum for providing the part of the type specimen of chlormagaluminite for our study and Mikhail M. Moiseev for the photographing of this specimen. We are grateful to reviewers for their valuable comments.

Conflicts of Interest: The authors declare no conflict of interest.

References

1. Mills, S.J.; Christy, A.G.; Génin, J.-M.R.; Kameda, T.; Colombo, F. Nomenclature of the hydrotalcite supergroup: Natural layered double hydroxides. *Mineral. Mag.* **2012**, *76*, 1289–1336.
2. Aşçı, Y.S. Removal of textile dye mixtures by using modified Mg-Al-Cl layered double hydroxide (LDH). *J. Dispers. Sci. Technol*. **2017**, *38*, 923–929.
3. Hongo, T.; Wakasa, H.; Yamazaki, A. Synthesis and adsorption properties of nanosized Mg-Al layered double hydroxides with Cl^-, NO_3^- or SO_4^{2-} as interlayer anion. *Mater. Sci. Pol*. **2011**, *29*, 86–91.
4. Huang, P.-P.; Cao, C.-Y.; Wei, F.; Sun, Y.-B.; Song, W.-G. MgAl layered double hydroxides with chloride and carbonate ions as interlayer anions for removal of arsenic and fluoride ions in water. *RSC Adv*. **2015**, *5*, 10412–10417.
5. Islam, M.; Patel, R. Synthesis and physicochemical characterization of Zn/Al chloride layered double hydroxide and evaluation of its nitrate removal efficiency. *Desalination* **2010**, *256*, 120–128.
6. Mahjoubi, F.Z.; Khalidi, A.; Cherkaoui, O.; Elmoubarki, R.; Abdennouri, M.; Barka, N. Treatment of textile effluents by chloride-intercalated Zn-, Mg- and Ni-Al layered double hydroxides. *J. Water Reuse Desalin.* **2017**, *7*, 307–318.
7. Yue, X.; Liu, W.; Chen, Z.; Lin, Z. Simultaneous removal of Cu(II) and Cr(VI) by Mg-Al-Cl layered double hydroxide and mechanism insight. *J. Environ. Sci*. **2017**, *53*, 16–26.
8. Curtius, H.; Kattilparampil, Z. Sorption of iodine on Mg-Al-layered double hydroxide. *Clay Miner.* **2005**, *40*, 455–461.
9. Curtius, H.; Kaiser, G.; Rozov, K.; Neumann, A.; Dardenne, K.; Bosbach, D. Preparation and characterization of Fe-, Co-, and Ni-containing Mg-Al-Layered double hydroxides. *Clays Clay Miner*. **2013**, *61*, 424–439.
10. Curtius, H.; Ufer, K. Eu incorporation behavior of a Mg-Al-Cl layered double hydroxide. *Clays Clay Miner*. **2007**, *55*, 354–360.
11. Shan, D.; Cosnier, S.; Mousty, C. Layered double hydroxides: An attractive material for electrochemical biosensor design. *J. Anal. Chem.* **2003**, *75*, 3872–3879.
12. Polese, D.; Mattoccia, A.; Giorgi, F.; Pazzini, L.; Ferronea, A.; Di, Giamberardino, L.; Maiolo, L.; Pecora, A.; Convertino, A.; Fortunato, G.; et al. Layered double hydroxides intercalated with chlorine used as low temperature gas sensors. *Procedia Eng*. **2015**, *120*, 1175–1178.
13. Cunha, V.R.; de Souza, R.B.; da Fonseca, Martins, A.M.; Koh, I.H.; Constantino, V.R. Accessing the biocompatibility of layered double hydroxide by intramuscular implantation: Histological and microcirculation evaluation. *Sci. Rep*. **2016**, *6*, 1–10, doi:10.1038/srep30547.
14. Conterosito, E.; Gianotti, V.; Palin, L.; Boccaleri, E.; Viterbo, D.; Milanesio, M. Facile preparation methods of hydrotalcite layered materials and their structural characterization by combined techniques. *Inorg. Chim. Acta* **2018**, *470*, 36–50.
15. Hu, G.; Wang, N.; O'Hare, D.; Davisa, J. Synthesis of magnesium aluminium layered double hydroxides in reverse microemulsions. *J. Mater. Chem*. **2017**, *17*, 2257–2266.
16. Isupov, V.P.; Chupakhina, L.E.; Mitrofanova, R.P. Mechanochemical Synthesis of Double Hydroxides. *J. Mater. Synth. Process*. **2000**, *8*, 251–253.
17. Oestreicher, V.; Jobbágy, M. One pot synthesis of $Mg_2Al(OH)_6Cl{\cdot}1.5H_2O$ layered double hydroxides: The epoxide route. *Langmuir* **2013**, *29*, 12104–12109.

18. Poonoosamy, J.; Brandt, F.; Stekiel, M.; Kegler, P.; Klinkenberg, M.; Winkler, B.; Vinograd, V.; Bosbach, D.; Deissmann, G. Zr-containing layered double hydroxides: Synthesis, characterization and evaluation of thermodynamic properties. *Appl. Clay Sci.* **2018**, *151*, 54–65.
19. Xu, Z.P.; Lu, G.Q. Hydrothermal synthesis of layered double hydroxides (LDHs) from mixed MgO and Al_2O_3: LDH formation mechanism. *Chem. Mater.* **2005**, *17*, 1055–1062.
20. Xu, J.; Zhang, L.; Li, D.; Zhao, J.; Hou, W. Synthesis of Mg_2Al-Cl layered double hydroxide nanosheets in a surfactant-free reverse microemulsion. *Colloid Polym. Sci.* **2013**, *291*, 2515–1521.
21. Feoktistov, G.D.; Ivanov, S.I.; Kashaev, A.A.; Klyuchnskii, L.N.; Taskina, N.G.; Ushchapovskaya, Z.F. Occurrence of chlormanasseite in the USSR. *Int. Geol. Rev*. **1979**, *21*, 1229–1232.
22. Kashaev, A.A.; Feoktistov, G.D.; Petrova, S.V. Chlormagaluminite, $(Mg,Fe^{2+})_4Al_2(OH)_{12}(Cl,1/2CO_3)_2(H_2O)_2$, a new mineral of the manasseite-sjögrenite group. *Zapiski VMO (Proc. Soviet Miner. Soc.)* **1982**, *111*, 121–127. (In Russian)
23. Kashaev, A.A.; Feoktistov, G.D.; Petrova, S.V. Chlormagaluminite, $(Mg,Fe^{2+})_4Al_2(OH)_{12}(Cl,1/2CO_3)_2(H_2O)_2$, a new mineral of the manasseite-sjögrenite group. *Int. Geol. Rev.* **1983**, *25*, 848–853.
24. Kashaev, A.A.; Kanashenok, S.V.; Rozhdestevenskaya, I.V. *Structure Refinement of Chlormagaluminite. Crystal Chemistry and X-ray Diffraction of Minerals*; Frank-Kamenetsky, V.A., Ed.; Nauka: Leningrad (USSR), Russia, 1987; pp. 101–105. (In Russian)
25. Ennadi, A.; Legrouri, A.; De Roy, A.; Besse, J.P. X-Ray diffraction pattern simulation for thermally treated [Zn-Al-Cl] layered double hydroxide. *Solid State Chem*. **2000**, *152*, 568–572.
26. Lombardo, G.M.; Pappalardo, G.C.; Punzo, F.; Costantino, F.; Costantino, U.; Sisani, M. A novel integrated X-ray powder diffraction (XRPD) and molecular dynamics (MD) approach for modeling Mixed-Metal (Zn, Al) layered double hydroxides (LDHs). *Eur. J. Inorg. Chem*. **2005**, *2005*, 5026–5034.
27. Bruker AXS. *APEX2*; Version 2014.11-0; Bruker AXS: Madison, WI, USA, 2014.
28. CrysAlis, P.R.O. Agilent Technologies Ltd.: Yarnton, UK, 2014.
29. Sheldrick, G.M. Crystal structure refinement with SHELXL. *Acta Crystallogr. Sect. C* **2015**, *71*, 3–8.
30. Momma, K.; Izumi, F. VESTA 3 for three-dimensional visualization of crystal, volumetric and morphology data. *J. Appl. Crystallogr*. **2011**, *44*, 1272–1276.
31. Zhitova, E.S.; Krivovichev, S.V.; Pekov, I.V.; Greenwell, H.C. Crystal chemistry of natural layered double hydroxides. 5. Single-crystal structure refinement of hydrotalcite, $[Mg_6Al_2(OH)_{16}](CO_3)(H_2O)_4$. *Mineral. Mag.* **2019**, doi:10.1180/mgm.2018.145.
32. Britvin, S.N.; Dolivo-Dobrovolsky, D.V.; Krzhizhanovskaya, M.G. Software for processing of X-ray powder diffraction data obtained from the curved image plate detector of Rigaku RAXIS Rapid II diffractometer. *Zapiski RMO (Proc. Russian Miner. Soc.)* **2017**, *146*, 104–107. (In Russian)
33. Bruker AXS. *TopasV4.2: General Profile and Structure Analysis Software for Powder Diffraction Data*; Bruker AXS: Karlsruhe, Germany, 2009.
34. Zhitova, E.S.; Krivovichev, S.V.; Yakovenchuk, V.N.; Ivanyuk, G.Y.; Pakhomovsky, Y.A.; Mikhailova, J.A. Crystal chemistry of natural layered double hydroxides: 4. Crystal structures and evolution of structural complexity of quintinite polytypes from the Kovdor alkaline-ultrabasic massif, Kola peninsula, Russia. *Mineral. Mag*. **2018**, *82*, 329–346.
35. Theiss, F.; López, A.; Frost, R.L.; Scholz, R. Spectroscopic characterisation of the LDH mineral quintinite $Mg_4Al_2(OH)_{12}CO_3{\cdot}3H_2O$. *Spectrochim. Acta Part A Mol. Biomol. Spectrosc.* **2015**, *150*, 758–764.
36. Speck, A. Single-crystal structure validation with the program PLATON. *J. Appl. Crystallogr*. **2003**, *36*, 7–13.
37. Zhitova, E.S.; Pekov, I.V.; Chukanov, N.V.; Yapaskurt, V.O.; Bocharov, V.N. Minerals of the stichtite-pyroaurite-iowaite-woodallite system from serpentinites of Terektinsky range, Altay Mountains, Russia. *Russ. Geol. Geoph.* **2019**, in press.
38. Braithwaite, R.S.W.; Dunn, P.J.; Pritchard, R.G.; Paar, W.H. Iowaite, a re-investigation. *Mineral. Mag.* **1994**, *58*, 79–85.
39. Kohls, D.W.; Rodda, J.L. Iowaite, a new hydrous magnesium hydroxide-ferric oxychloride from the Precambrian of Iowa. *Am. Mineral*. **1967**, *52*, 1261–1271.
40. Grguric, B.A.; Madsen, I.C.; Pring, A. Woodallite, a new chromium analog of iowaite from the Mount Keith nickel deposit, Western Australia. *Mineral. Mag.* **2001**, *65*, 427–435.
41. Mikhailenko, D.S.; Korsakov, A.V.; Rashchenko, S.V.; Seryotkin, Y.V.; Belakovskiy, D.I.; Golovin, A.V. Kuliginite, a new hydroxychloride mineral from the Udachnaya kimberlite pipe, Yakutia: Implications for low-temperature hydrothermal alteration of the kimberlites. *Am. Mineral*. **2018**, *103*, 1435–1444.

42. Mazurov, M.P.; Korneva, T.A.; Zhitova, L.M.; Istomin, V.E.; Palchik, N.A.; Stopovskaya, V.N.; Titov, A.T. Iowaite from Korshunovskoe deposit (the Siberian platform). *Zapiski RMO (Proc. Russian Miner. Soc.)* **2000**, *129*, 80–85.
43. Evseev, A.A. Siberia's Crystals and Symmetry in the Distribution of Occurrences of Minerals. *World Stones* **1973**, *1*, 11–20.
44. Melchiorre, E.B.; Bottrill, R.; Huss, G.R.; Lopez, A. Conditions of stichtite ($Mg_6Cr_2(OH)_{16}[CO_3]\cdot 4H_2O$) formation and its geochemical and isotope record of early phanerozoic serpentinizing environments. *Geochim. Cosmochim. Acta* **2017**, *197*, 43–61.
45. Guinier, A.; Bokij, G.B.; Boll-Dornberger, K.; Cowley, J.M.; Durovic, S.; Jagodzinski, H.; Krishna, P.; DeWolff, P.M.; Zvyagin, B.B.; Cox, D.E.; et al. Nomenclature of polytype structures. Report of the International Union of Crystallography ad-hoc committee on the Nomenclature of disordered, modulated and polytype structures. *Acta Crystallogr.* **1984**, *A40*, 399–404.
46. Bookin, A.S.; Drits, V.A. Polytype diversity of the hydrotalcite-like minerals. I. Possible polytypes and their diffraction patterns. *Clays Clay Miner*. **1993**, *41*, 551–557.
47. Britto, S.; Kamath, P.V. Structure of bayerite-based lithium-aluminum layered double hydroxides (LDHs): Observation of monoclinic symmetry. *Inorg. Chem*. **2009**, *48*, 11646–11654.
48. Britto, S.; Kamath, P.V. Polytypism in the lithium-aluminum layered double hydroxides: The $[LiAl_2(OH)_6]^+$ layer as a structural synthon. *Inorg. Chem*. **2011**, *50*, 5619–5627.
49. Britto, S.; Thomas, G.S.; Kamath, P.V.; Kannan, S. Polymorphism and structural disorder in the carbonate containing layered double hydroxide of Li with Al. *J. Phys. Chem*. **2008**, *112*, 9510–9515.
50. Sissoko, I.; Iyagba, E.T.; Sahai, I.; Biloen, P. Anion intercalation and exchange in $Al(OH)_3$-derived compounds. *Solid State Chem*. **1985**, *60*, 283–288.
51. Allmann, R. The crystal structure of pyroaurite. *Acta Crystallogr.* **1968**, *B24*, 972–977.
52. Ingram, L. and Taylor, H.F.W. The crystal structures of sjoegrenite and pyroaurite. *Mineral. Mag*. **1967**, *36*, 465–479.
53. Zhitova, E.S.; Ivanyuk, G.Y.; Krivovichev, S.V.; Yakovenchuk, V.N.; Pakhomovsky, Y.A.; Mikhailova, Y.A. Crystal Chemistry of Pyroaurite from the Kovdor Pluton, Kola Peninsula, Russia, and the Långban Fe-Mn deposit, Värmland, Sweden. *Geol. Ore Deposits*. **2017**, *59*, 652–661.
54. Krivovichev, S.V.; Yakovenchuk, V.N.; Zhitova, E.S.; Zolotarev, A.A.; Pakhomovsky, Y.A.; Ivanyuk, G.Y. Crystal chemistry of natural layered double hydroxides. 1. Quintinite-2*H*-3*c* from the Kovdor alkaline massif, Kola peninsula, Russia. *Mineral. Mag*. **2010**, *74*, 821–832.
55. Krivovichev, S.V.; Yakovenchuk, V.N.; Zhitova, E.S.; Zolotarev, A.A.; Pakhomovsky, Y.A.; Ivanyuk, G.Y. Crystal chemistry of natural layered double hydroxides. 2. Quintinite-1*M*: First evidence of a monoclinic polytype in M^{2+}-M^{3+} layered double hydroxides. *Mineral. Mag.* **2010**, *74*, 833–840.
56. Krivovichev, S.V.; Yakovenchuk, V.N.; Zhitova, E.S. Natural double layered hydroxides: Structure,chemistry, and information storage capacity. In *Minerals as Advanced Materials II*; Krivovichev, S.V., Ed.; Springer: Berlin/Heidelberg, Germany, 2012; pp. 87–102.
57. Zhitova, E.S.; Yakovenchuk, V.N.; Krivovichev, S.V.; Zolotarev, A.A.; Pakhomovsky, Y.A.; Ivanyuk, G.Y. Crystal chemistry of natural layered double hydroxides. 3. The crystal structure of Mg, Al-disordered quintinite-2*H*. *Mineral. Mag*. **2010**, *74*, 841–848.
58. Zhitova, E.S.; Popov, M.P.; Krivovichev, S.V.; Zaitsev, A.N.; Vlasenko, N.S. Quintinite-1*M* from the Mariinskoe deposit, Ural Emerald Mines, Southern Urals, Russia. *Geol. Ore Deposits*. **2017**, *59*, 745–751.
59. Mills, S.J.; Whitfield, P.S.; Kampf, A.R.; Wilson, S.A.; Dipple, G.M.; Raudsepp, M.; Favreau, G. Contribution to the crystallography of hydrotalcites: The crystal structures of woodallite and takovite. *J. Geosci*. **2012**, *58*, 273–279.
60. Lozano, R.P.; Rossi, C.; La Iglesia, A.; Matesanz, E. Zaccagnaite-3*R*, a new Zn-Al hydrotalcite polytype from El Soplao cave (Cantabria, Spain). *Am. Mineral*. **2012**, *97*, 513–523.